

# Transforming carbon nanotubes by silylation: An *ab initio* study

Kiseok Chang, Savas Berber, and David Tománek

*Physics and Astronomy Department, Michigan State University, East Lansing, Michigan 48824-2320, USA*

(Dated: July 22, 2021)

We use *ab initio* density functional calculations to study the chemical functionalization of single-wall carbon nanotubes and graphene monolayers by silyl ( $\text{SiH}_3$ ) radicals and hydrogen. We find that silyl radicals form strong covalent bonds with graphene and nanotube walls, causing local structural relaxations that enhance the  $sp^3$  character of these graphitic nanostructures. Silylation transforms all carbon nanotubes into semiconductors, independent of their chirality. Calculated vibrational spectra suggest that specific frequency shifts can be used as a signature of successful silylation.

PACS numbers: 81.07.De, 61.46.-w, 68.65.-k, 73.63.Fg

Carbon nanotubes[1] have evolved into one of the most intensively studied one-dimensional nanostructures. They owe their success in the nanotechnology field to a unique combination of atomic-scale perfection, structural stability, beneficial thermal and electrical properties[1]. Their usefulness as molecular nanowires is hindered by two main limitations. First, reproducible formation of contacts with a well-defined geometry and electronic properties is difficult, since most materials do not wet the surface of the inert nanotube, but rather bond to ill-defined unterminated ends, causing large variations in the contact resistance[2]. Even more important is the fact that the conductance of carbon nanotubes depends sensitively on the precise way a graphene layer is rolled up into the tubular structure, identified by the chiral index  $(n, m)$ [3, 4, 5]. Since it is currently impossible to produce nanotubes with a unique chiral index, even samples with a narrow diameter range necessarily contain a mixture of metallic and semiconducting nanotubes, reducing their usefulness in quantum devices.

Here we propose that the recently[6] achieved chemical functionalization of carbon nanotubes by silyl groups bears promise for the nanotube walls to form strong, well-defined bonds to a surrounding matrix, and for the majority of nanotubes to convert into semiconducting nanowires. Using *ab initio* calculations, we demonstrate that silyl ( $-\text{SiH}_3$ ) radicals form strong covalent bonds with the surface of nanotubes and graphene. Since silylation introduces a partial  $sp^3$  character into the  $sp^2$  graphitic network, it opens up the fundamental band gap and converts all carbon nanotubes to semiconductors. We show that successful silylation of nanotubes can be verified experimentally by monitoring specific changes in the vibrational spectra[6].

The selection of silyl radicals as functional groups has been motivated by the success of silane chemistry in establishing strong, covalent bonds between polymers and inorganic matter[7]. The rich silane chemistry[8] is likely to provide ways to modify silyl radicals bonded to the nanotube wall in order to optimize covalent bonding of nanotube walls to many materials, including silicon. To our knowledge, there has been no prior theoretical study

of the silyl-nanotube interaction and the effect of silylation on the nanotube properties.

In order to determine, whether silyl radicals may covalently attach to nanotubes and thereby modify their conductance properties in a desirable way, we used *ab initio* calculations to determine the equilibrium geometry, total energy and electronic structure of silylated nanotubes. Our calculations are based on the density functional theory (DFT) within the local density approximation (LDA). We used the Perdew-Zunger [9] parameterized exchange-correlation functional, as implemented in the SIESTA code [10], and a double- $\zeta$  polarized basis localized at the atomic sites. The valence electrons were described by norm-conserving Troullier-Martins pseudopotentials [11] in the Kleinman-Bylander factorized form [12].

In our calculations, we considered the products of the dissociative adsorption of silane,  $\text{SiH}_4 \rightarrow \text{SiH}_3(\text{ad}) + \text{H}(\text{ad})$ , yielding silyl radicals and hydrogen atoms chemisorbed on graphene and carbon nanotubes at different coverages. We obtained results for carbon nanotubes of different diameters, with chiral indices ranging from  $(4, 4)$  to  $(18, 0)$ . To describe isolated nanotubes while using periodic boundary conditions, we arranged them on a tetragonal lattice with a large inter-wire separation of 22 Å. Depending on the  $\text{SiH}_3$  coverage and the chiral index, we used supercells containing up to 4 primitive unit cells in the tube direction[13] and sampled the Brillouin zone of these 1D structures by at least 7 k points. We limited the range of the localized orbitals in such a way that the energy shift caused by their spatial confinement was no more than 50 meV[14]. The charge density and the potentials were determined on a real-space grid with a mesh cutoff energy of 200 Ry, which was sufficient to achieve a total energy convergence of better than 0.1 meV/atom.

When calculating the vibrational spectrum of pristine and silylated nanotubes, we first optimized the reference structure to a high precision, with residual forces not exceeding 0.04 eV/Å. The high mesh cutoff energy value guarantees that the forces are translationally invariant. To obtain a good estimate of the Hessian matrix in the harmonic limit, we displaced atoms in the positive and

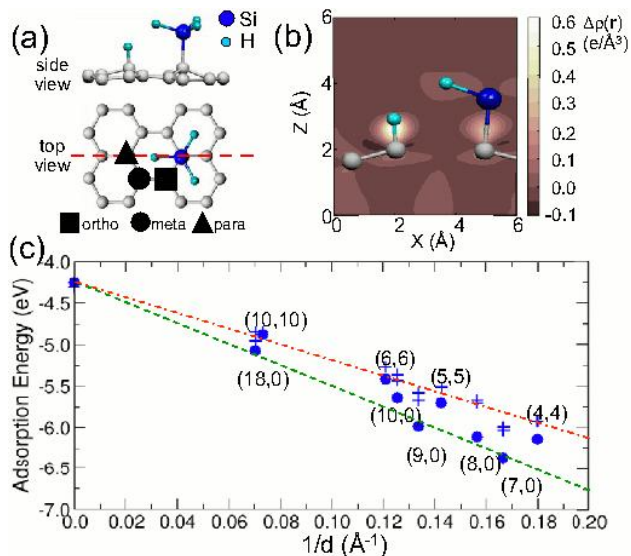


FIG. 1: (Color online) Bonding of SiH<sub>3</sub> and H to graphitic carbon. (a) Equilibrium adsorption geometry on graphene in side view (top panel) and top view (bottom panel). (b) Charge density difference  $\Delta\rho(r) = \rho(\text{SiH}_3 + \text{H}/\text{graphene}) - \rho(\text{SiH}_3) - \rho(\text{H}) - \rho(\text{graphene})$ , displayed in the plane indicated by the dashed line in (a). (c) Adsorption energy  $E_{ad}(\text{SiH}_3+\text{H})$  on carbon nanotubes as a function of the inverse tube diameter  $1/d$ .

negative direction along each axis by the small amount of 0.01 Å and determined the forces analytically. With these numerical precautions and limitations of the LDA force field, we found our frequencies to be dependable with the accuracy of down to few inverse centimeters. We also found our LDA-value[15] for the G-band frequency of 1630 cm<sup>-1</sup> to agree much better with the experimental value[16] of 1580 cm<sup>-1</sup> than previous LDA calculations[17].

We first considered co-adsorption of SiH<sub>3</sub> and H on graphene, a good model for a wide-diameter carbon nanotube. Our calculations suggest that both silyl and hydrogen preferentially adsorb on-top of carbon atoms, where they interact with the initially unfilled C2p<sub>z</sub> orbital. We found a weak mutual attraction between silyl and hydrogen, mediated by the graphene substrate. The different adsorption geometries in neighboring adsorption sites are indicated schematically in Fig. 1(a). For an isolated silyl-hydrogen pair, we distinguished the *ortho* geometry with the adsorbates adjacent from the *para* arrangement with the adsorbates on opposite corners of a single C<sub>6</sub> ring. In the *meta* arrangement, the adsorbates are neither adjacent nor opposite to each other on a single C<sub>6</sub> ring. Defining the adsorption energy  $E_{ad}(\text{SiH}_3+\text{H})$  as the energy to adsorb SiH<sub>3</sub> and H from the vacuum, we find  $E_{ad} = -4.25$  eV for *ortho*,  $-3.57$  eV for *meta*, and  $-4.31$  eV for *para* geometry. In view of the fact that the adsorption energy of a hydrogen atom on graphene is close to  $-1.4$  eV[18], we conclude that the bond strength

between the silyl radical and graphene is unusually large, exceeding 2 eV.

We find that the SiH<sub>4</sub>(ad)→SiH<sub>3</sub>(ad)+H(ad) dissociation on graphene, associated with a local pyramidalization of the initially planar graphene near the adsorption site, occurs with an energy barrier of  $\approx 1.5$  eV in the *para* arrangement. The pyramidalization seen in the optimum adsorption geometry, shown in side view in Fig. 1(a), indicates a local change of the bonding character from *sp*<sup>2</sup> to *sp*<sup>3</sup>, so that initially inert planar graphene is transformed into a reactive substrate capable of forming covalent bonds with adsorbates. The nature of the adsorption bond can be best seen by inspecting the charge density difference  $\Delta\rho$ , representing the charge redistribution in the system upon adsorption. The spatial distribution of  $\Delta\rho(r)$  for silyl and hydrogen adsorbed on graphene in the *para* arrangement is shown in Fig. 1(b) in a plane normal to the substrate. We observe no charge flow between adsorbate and substrate, but rather a moderate charge accumulation in the Si-C and H-C bond regions, indicating the formation of covalent bonds.

In contrast to graphene, the finite surface curvature of pristine nanotubes introduces partial *sp*<sup>3</sup> character, making these systems more reactive. This is best illustrated by plotting the adsorption energy  $E_{ad}(\text{SiH}_3+\text{H})$  as a function of the nanotube diameter in Fig. 1(c) for one SiH<sub>3</sub> and one H per supercell[13]. As the *sp*<sup>3</sup> character increases with decreasing nanotube diameter, there is a decreasing energy cost to distort the substrate in order to optimize the adsorption bond, thus making adsorption more exothermic. Also at high coverages, we expect the adsorption bonds to be stronger on the average than at low coverages. In contrast to the first adsorbates in the supercell that introduce local substrate distortion, bonding of additional adsorbates benefits energetically from the previously enhanced *sp*<sup>3</sup> bonding character. Depending on the adsorption arrangement within the supercell, we have found a strengthening of the average adsorption bond by up to 0.4 eV when increasing the coverage from one to three SiH<sub>3</sub> and H units per supercell.

Our results for the most stable adsorption arrangement on an (n, m) nanotube are given by solid data points, and less stable arrangements by the crosses in Fig. 1(c). With respect to our graphene results, the adsorption energy differences between the *ortho*, *meta* and *para* arrangements in (n, m) nanotubes may change by up to a few tenths of an eV per supercell, thus changing the most favored adsorption arrangement. At nonzero coverages, we find that silyls and hydrogens prefer to form lines in axial direction, thus minimizing the strain energy in the substrate. Among the systems investigated here, we found silyl and hydrogen to bond more strongly to zigzag than to armchair nanotubes due to differences in the pyramidalization strain.

Having established that silyl radicals and hydrogen form strong covalent bonds with nanotubes, we next in-

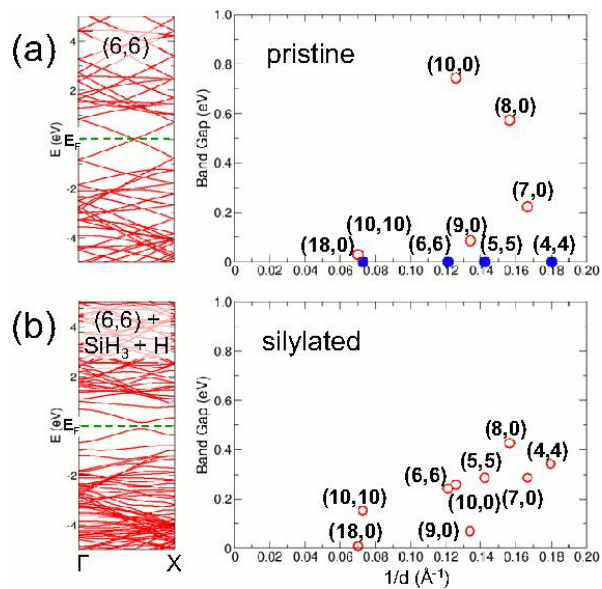


FIG. 2: (Color online) Electronic structure of (a) pristine and (b) silylated carbon nanotubes. The left panels display the effect of silylation on the band structure of the (6,6) nanotube. The right panels show the fundamental band gap  $E_g$  in nanotubes as a function of the inverse tube diameter  $1/d$ . Data for metallic nanotubes are given by solid symbols, those for semiconducting nanotubes by open symbols.

investigate the effect of chemisorption on the electronic structure of carbon nanotubes. As mentioned earlier, the fundamental band gap of pristine carbon nanotubes varies strongly with the chiral index  $(n, m)$ [3, 4, 5]. In density functional calculations, the band gap value is known to be underestimated significantly. Consequently, the range of band gap values in nanotubes should be even larger than what is suggested by the DFT results for pristine nanotubes in the right panel of Fig. 2(a). In a sample with a random distribution of chiral indices  $(n, m)$ , we expect one third of nanotubes to be metallic[3, 4, 5]. For better visual impact, metallic nanotubes are represented by solid data points and semiconducting nanotubes by open data points in the right panel of Fig. 2(a). The band structure  $E(k)$  of the pristine (6,6) armchair carbon nanotube is shown in the left panel of Fig. 2(a) as a representative for other metallic nanotubes.

The effect of silylation on the electronic structure of carbon nanotubes is shown in Fig. 2(b). Comparing the calculated band gaps in the silylated and pristine nanotubes in the right panels of Fig. 2, we conclude that silylation has converted all nanotubes to semiconductors and narrowed down the range of their fundamental band gaps. Details of silylation-related changes in the electronic structure can be best seen when comparing the electronic structure of the pristine and the silylated (6,6) nanotube in the left panels of Fig. 2. Whereas the metallic character of the pristine system stems from the crossing of two linear bands at the Fermi level, enhancing

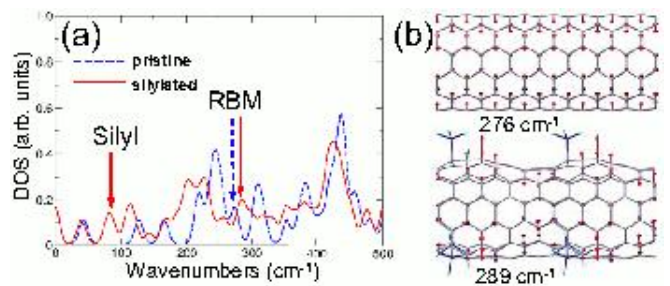


FIG. 3: (Color online) Effect of silylation on the vibrations of the (6,6) carbon nanotube. (a) Low-frequency range of the vibrational spectrum. (b) Schematic of the radial breathing mode (RBM) in the pristine and silylated nanotube.

the  $sp^3$  character by silylation opens up a direct band gap in this system. Only in systems, where the number of H and SiH<sub>3</sub> adsorbates per unit cell is not the same, a non-bonding low-dispersion band appears in the band gap near  $E_F$ . This impurity band is spin polarized and localized near the adsorbates.

Obviously, the band gap of a given nanotube will change with changing  $sp^3$  character[19], which depends on the adsorption geometry and the adsorbate coverage. Our band gap results in the right panel of Fig. 2(b) are for a low coverage of one SiH<sub>3</sub> and H per supercell[13] of the pristine nanotube. Since the  $sp^3$  character should increase with rising silyl coverage, and since DFT underestimates the fundamental band gap, our results in the right panel of Fig. 2(b) are to be considered a lower bound on band gaps in silylated nanotubes.

Successful silylation of nanotubes can be verified experimentally by inspecting the vibrational spectra as a specific signature of silyl-nanotube bonds. Reported Raman spectra of silylated carbon nanotubes[6] suggest that the dominant effect of silylation is the modification of mode intensities. No frequency shifts specifically related to silylation have been observed, suggesting that the effect of silylation may be comparable to that of bundling[6]. In the following, we determine the vibrational spectra of pristine and silylated nanotubes in order to identify a spectroscopic signature of the silyl-nanotube bond.

We have studied the vibrational spectra of (6,6) and (10,0) carbon nanotubes containing up to three silyls and hydrogens per supercell[13]. Upon silylation, we first expect the emergence of new vibrational modes in the nanotube, associated with Si-C and H-C stretch motion. Silylation furthermore modifies the vibrational modes of the pristine nanotube due to adsorbate-related deformations and local stress, as well as the attachment of heavy SiH<sub>3</sub> ligands.

Comparing the vibrational spectra of (6,6) and (10,0) nanotubes, we find the general trends for silylation-related changes to be chirality independent, and frequency shifts to be generally less than 20  $\text{cm}^{-1}$ . The

vibrational spectra of a pristine and a silylated (6,6) carbon nanotube, with three silyls and hydrogens in the *ortho* arrangement forming a ring within the 9.9 Å long supercell[13], are compared to each other in Fig. 3(a). In the low-frequency part of the spectrum, silylated nanotubes exhibit a mode at  $\approx 80 \text{ cm}^{-1}$ , caused by the wagging motion of the chemisorbed radicals. Other modes induced by silylation include the high-frequency H-Si stretch in  $\text{SiH}_3$  at  $2000 \text{ cm}^{-1}$  and the H-C stretch of the adsorbed hydrogens at  $2800 \text{ cm}^{-1}$ .

A vibration mode unique to carbon nanotubes is the  $A_{1g}$  radial breathing mode (RBM), shown schematically in the top panel of Fig. 3(b). As seen in Fig. 3(a), this mode occurs at  $276 \text{ cm}^{-1}$  in the pristine (6,6) nanotube. Even though the RBM mode is not well defined in partly silylated nanotubes, a closely related mode, shown in the bottom panel of Fig. 3(b), occurs at the higher frequency of  $289 \text{ cm}^{-1}$  in the silylated nanotube. Similar RBM up-shifts have been reported in pristine tubes and traced back to hydrostatic pressure[20, 21] or stress induced by inter-tube interaction[22]. We find an up-shift of RBM-like modes at lower coverages, when the axial distance between adsorbed silyl radicals is large, and a down-shift at high coverages, when most carbon atoms are covalently bonded to a silyl. Much of this trend can be understood and reproduced by considering carbon atoms connected to silyls as virtual ‘heavy’  $^{43}\text{C}$  ‘isotopes’ within the pristine nanotube. In the low-coverage regime considered in Fig. 3(b), the heavy carbons move radially out of phase with the other carbons, causing a frequency up-shift. At high coverages, all carbons are subject to the usual radial breathing motion with the frequency down-shifted by the isotope effect.

The high-frequency tangential mode, also known as the G band, is down-shifted in the silylated nanotube to  $1619 \text{ cm}^{-1}$  from its initial value of  $1638 \text{ cm}^{-1}$  in the pristine (6,6) nanotube. This frequency shift is almost independent of the silyl coverage.

In conclusion, we used *ab initio* density functional calculations to study the chemical functionalization of single-wall carbon nanotubes and graphene monolayers by silyl radicals and hydrogen. We found that silyl radicals form strong covalent bonds with graphene and nanotube walls, causing local structural relaxations that enhance the  $sp^3$  character of these graphitic nanostructures. With the help of silane chemistry, nanotube walls may form strong, well-defined bonds to a surrounding matrix, facilitating the transition to carbon-silicon hybrid electronics. We found that silylation transforms all carbon nanotubes into semiconductors, independent of their chirality. Our calculated vibrational spectra suggest that specific frequency shifts can be used as a signature of successful silylation.

We acknowledge useful discussions with Yung-Doug Suh and Hee-Cheul Choi about silylation of carbon nanotubes and the assistance of Shinya Okano with nu-

merical calculations. This work was funded by the National Science Foundation under NSF-NSEC grant 425826 and NSF-NIRT grant ECS-0506309. Computational resources have been provided by the Michigan State University High Performance Computing Center.

- 
- [1] A. Jorio, M. Dresselhaus, and G. Dresselhaus, *Carbon Nanotubes: Advanced Topics in the Synthesis, Structure, Properties and Applications*, vol. 111 of *Topics in Applied Physics* (Springer, Berlin, 2008).
  - [2] N. Nemeč, D. Tomanek, and G. Cuniberti, *Phys. Rev. Lett.* **96**, 076802 (2006).
  - [3] J. W. Mintmire, B. I. Dunlap, and C. T. White, *Phys. Rev. Lett.* **68**, 631 (1992).
  - [4] R. Saito, M. Fujita, G. Dresselhaus, and M. S. Dresselhaus, *Appl. Phys. Lett.* **60**, 2204 (1992).
  - [5] N. Hamada, S. I. Sawada, and A. Oshiyama, *Phys. Rev. Lett.* **68**, 1579 (1992).
  - [6] T. Hemraj-Benny and S. S. Wong, *Chem. Mater.* **18**, 4827 (2006).
  - [7] K. Weissenbach and H. Mack, in *Functional Fillers for Plastics*, edited by M. Xanthos (WILEY-VCH, Weinheim, 2005), chapter 4, pp. 57–84.
  - [8] A. E. Pierce, *Silylation of organic compounds* (Pierce Chemical Company, Rockford, Illinois, 1968).
  - [9] J. P. Perdew and A. Zunger, *Phys. Rev. B* **23**, 5048 (1981).
  - [10] J. M. Soler, E. Artacho, J. D. Gale, A. García, J. Junquera, P. Ordejón, and D. Sánchez-Portal, *J. Phys: Condens. Matter* **14**, 2745 (2002).
  - [11] N. Troullier and J. L. Martins, *Phys. Rev. B* **43**, 1993 (1991).
  - [12] L. Kleinman and D. M. Bylander, *Phys. Rev. Lett.* **48**, 1425 (1982).
  - [13] We used supercells of comparable length, containing 4 primitive unit cells for armchair nanotubes and 2 primitive unit cells for zigzag nanotubes.
  - [14] E. Artacho, D. Sánchez-Portal, P. Ordejón, A. García, and J. M. Soler, *Phys. Stat. Sol.* **215**, 809 (1999).
  - [15] Whereas LDA provides a more consistent picture of bonding to  $sp^2$  carbons, the GGA force field sometimes achieves better agreement with experimental results. Our GGA value of  $1582 \text{ cm}^{-1}$  for the G-band frequency is in perfect agreement with the experimental value.
  - [16] A. C. Ferrari, J. C. Meyer, V. Scardaci, C. Casiraghi, M. Lazzeri, F. Mauri, S. Piscanec, D. Jiang, K. S. Novoselov, S. Roth, et al., *Phys. Rev. Lett.* **97**, 187401 (2006).
  - [17] S. Reich, C. Thomsen, and P. Ordejón, *Phys. Rev. B* **64**, 195416 (2001).
  - [18] G. Miller, J. Kintigh, E. Kim, P. Weck, S. Berber, and D. Tomanek, *J. Am. Chem. Soc.* **130**, 2296 (2008).
  - [19] L. Yang and J. Han, *Phys. Rev. Lett.* **85**, 154 (2000).
  - [20] S. Lefrant, I. Baltog, and M. Baibarac, *J. Raman Spectroscopy* **36**, 676 (2005).
  - [21] J. Sandler, M. S. P. Shaffer, A. H. Windle, M. P. Halsall, M. A. Montes-Morán, C. A. Cooper, and R. J. Young, *Phys. Rev. B* **67**, 035417 (2003).
  - [22] M. S. Dresselhaus and P. C. Eklund, *Adv. Phys.* **49**, 705 (2000).